Helical Mode Lung 4D-CT Reconstruction Using Bayesian Model

Tiancheng He, Zhong Xue*, Paige L. Nitsch, Bin S. Teh, and Stephen T. Wong

The Methodist Hospital Research Institute, The Methodist Hospital,
Weill Cornell Medical College, Houston, TX, US
zxue@tmhs.org

Abstract. 4D computed tomography (CT) has been widely used for treatment planning of thoracic and abdominal cancer radiotherapy. Current 4D-CT lung image reconstruction methods rely on respiratory gating to rearrange the large number of axial images into different phases, which may be subject to external surrogate errors due to poor reproducibility of breathing cycles. New image-matching-based reconstruction works better for the cine mode of 4D-CT acquisition than the helical mode because the table position of each axial image is different in helical mode and image matching might suffer from bigger errors. In helical mode, not only the phases but also the un-uniform table positions of images need to be considered. We propose a Bayesian method for automated 4D-CT lung image reconstruction in helical mode 4D scans. Each axial image is assigned to a respiratory phase based on the Bayesian framework that ensures spatial and temporal smoothness of surfaces of anatomical structures. Iterative optimization is used to reconstruct a series of 3D-CT images for subjects undergoing 4D scans. In experiments, we compared visually and quantitatively the results of the proposed Bayesian 4D-CT reconstruction algorithm with the respiratory surrogate and the image matching-based method. The results showed that the proposed algorithm yielded better 4D-CT for helical scans.

Keywords: Bayesian estimation, respiratory motion, 4D-CT reconstruction.

1 Introduction

4D-CT has been widely used for radiation therapy planning of lung cancer for defining the clinical target volume (CTV) and planning target volume (PTV) to ensure that the radiation dose covers CTV, is within PTV, and does not damage neighboring critical tissues during respiratory cycles [1, 2]. 4D-CT scanning captures a large number of axial images during multiple breathing cycles using cine or helical modes, and reconstructs them to a series of 3D-CT images [3]. The cine mode captures multiple axial images in respiratory cycles at each table position; while the helical mode performs the scans when the table is slowly and continuously moving.

Efforts have been made to either using respiratory sensors such as gating and optical tracking to capture detailed respiratory motion patterns or using image computing

* Corresponding author.

K. Mori et al. (Eds.): MICCAI 2013, Part III, LNCS 8151, pp. 33–40, 2013.

methods to retrospectively improve the image sorting. Traditionally, using surrogate respiratory signals from a chest height marker, a strain gauge or a spirometer [4], respiratory cycles are detected and divided into a number of respiratory phases. Then, the synchronized axial images are rearranged to reconstruct the serial 3D images. However, because of the lack of reproducibility of breathe cycles, such gating signals appear to be not exactly periodical and may miss group some axial images, resulting discontinuity of anatomical structures in the images [5-7]. Recent studies have attempted to reconstruct 4D-CT through image computing in the cine mode [8-11]. For helical mode, since each axial image has a different table position, such additional variable should be considered in the reconstruction, and few works have been reported in the literature. As more helical 4D scans are being used in radiotherapy planning, it is highly desirable to study the methods for its image reconstruction.

This paper proposes an automated 4D-CT reconstruction algorithm for helical scanning based on the Bayesian framework, referred to as Bayesian 4D-CT reconstruction. The objective for lung 4D-CT image reconstruction is to preserve the anatomical structures at each time-point, while the image sequence reflects underlying respiratory motion. Spatial and temporal smoothness of certain surfaces of anatomical structures can be used as constraints in the reconstruction. In the Bayesian 4D-CT reconstruction algorithm, image sorting is jointly estimated with an underlying ideal image sequence whose surface's spatial-temporal properties are subject to such smoothness constraints. A novel energy function is designed and formulated in the Bayesian framework, and the optimization is achieved by iteratively assigning axial images to their best phase, and at the same time, enforcing spatial-temporal surface smoothness. Finally, due to the nature of helical 4D scanning, the image and surface matching also takes into account the unequal inter-slice distances of axial images in each respiratory phase, and the final reconstructed images are generated using a cubic B-Spline-based interpolation.

In experiments, we used the images from thirty nine patients undergoing radiotherapy planning to validate the algorithm. The final reconstructed images were compared visually and quantitatively with the external surrogate-based reconstruction and the image matching-based method [10] that are currently used in radiotherapy planning. For quantitative comparison, we compared the spatial and temporal smoothness of the surfaces extracted from all the results. The results indicated that our method outperformed both methods: visualization of the CT images showed less artifacts, particularly in the regions close to the diaphragm; and quantitative results showed that the surfaces extracted from the resultant images were smoother, so there was less sudden bumps along the image boundaries.

2 Method

2.1 Algorithm Formulation

During the helical mode scanning, axial images are captured while the table is slowly and continuously moving. Depending on the slice thickness and the number of simultaneous slices the scanner can capture (e.g., multiple row detector CT), the table speed can be determined so that the axial images captured within a small position range cover an entire respiratory cycle. Using the synchronized surrogate respiratory signal

the axial images can be initially resorted to different respiratory phases, and each 3D image is formed by the axial images according to their table positions. The goal for the proposed Bayesian 4D-CT reconstruction algorithm is to assess such assignment and correct the miss grouped ones so that the 3D images at each phase preserve anatomical structures, and the 4D data reflect respiratory motion well. Thus, spatial and temporal smoothness of surfaces act as the key for enforcing this requirement. We used the smoothness constraint of chest surface to ensure the quality of the reconstructed images. The reason is that it is smoother compared to internal organs, and it is also possible to extend our algorithm to use computer vision-based method to track the chest surface. Suppose the set of all axial images is D, the chest surfaces of an underlying ideal image sequences are $R=\{R_1, R_2, \dots, R_K\}$, and R and D are independent, the goal of our reconstruction algorithm is to jointly estimate a new image series $S=\{s_1, s_2, \dots, s_K\}$ and the ideal surfaces R by maximizing the following joint posterior distribution, where K is number of respiratory phases in one breathing cycle:

$$P(S,R|D)=\frac{P(D|S)P(S,R)}{P(D)}. \tag{1}$$

The joint probability of S and R can be expressed as,

$$P(S,R)=P(S|R)P(R). \tag{2}$$

Combining Eq. (1) and Eq. (2), and assuming that the probability of the known axial image set D is 1 ($P(D)=1$), S and R can be estimated by

$$(S^*,R^*)=\text{argmax}\{P(S,R|D)\}=\text{argmax}\{P(D|S)P(S|R)P(R)\}. \tag{3}$$

When the probabilities are estimated using the Gibbs distribution, the maximization of the joint posterior distribution is equivalent to minimizing the energy function:

$$E(S,R)=E(D|S)+\alpha E(S|R)+\beta E(R). \tag{4}$$

α and β are the weighting factors. The first term $E(D|S)$ denotes the degree of matching between the serial image S and the observed data D, and it can be calculated by the normalized cross correlation (NCC) between the two image series:

$$E(D|S)=\sum_{k=1}^{K}-NCC(D_k,S_k). \tag{5}$$

The second term $E(S|R)$ stands for the degree of matching between S and R, with R as the underlying ideal surfaces. Here, $E(S|R)$ is defined by the distance between ideal surface R and the surfaces extracted from S,

$$E(S|R)=\sum_{k=1}^{K}\text{dist}(G(S_k),R_k), \tag{6}$$

where the distance dist() is calculated according to [12]. $G(S_k)$ represents the surface extracted from S_k. The third term of Eq. (4) represents the prior shape constraints of R. In this case, it consists of the spatial and temporal smoothness constraints of the chest surface series. Because it is not necessary to constrain the surface within each axial plane, we only need to consider the smoothness in z-direction as well as in the time-domain (between neighboring phases). Thus, $E(R)$ is calculated as:

$$E(R)=\frac{1}{K}\sum_{k=1}^{K}\frac{1}{|\Omega|}\sum_{\mathbf{v}}\left(\frac{\partial R_k(\mathbf{v})}{\partial z}\right)^2+\lambda\frac{1}{K-1}\sum_{k=1}^{K-1}\frac{1}{|\Omega|}\sum_{\mathbf{v}}\left(\mathbf{f}_{k+1}(\mathbf{v}+\mathbf{f}_k(\mathbf{v}))-\mathbf{f}_k(\mathbf{v})\right)^2, \tag{7}$$

where the first term is the average of the squared surface gradients along z-direction by considering the unequal slice distances, and the second term calculates the average of the temporal smoothness of the deformation field $\mathbf{f}_k, k=1,\dots,K-1$ across the

image sequence. λ is the tradeoff between them, and Ω is the surface point set of the lung image in phase k.

Compared to the maximizing a posteriori (MAP) formulation, the major difference of the proposed algorithm is that an intermediate ideal surface R is jointly estimated together with S. This helps facilitate the additional spatial and temporal anatomical constraints to the reconstructed 4D-CT images. Finally, after assigning each axial image into their phase by minimizing the energy function defined in Eq. (4), the slices of each phase are arranged according to their table positions. Because of the unequal slice distances, we then use a cubic B-Spline-based interpolation tool to resample them and reconstruct the 3D image sequences with equal slice distance.

2.2 Implementation

The optimization of the energy function in Eq. (4) can be implemented by alternatively calculating R and S. Given a series of N axial images (for lung imaging, N is more than 1000), we can first sort them into K (typically 10) phases based on the surrogate signals, which gives the current data observation D. We use D as the initialization of S and iteratively perform the following two optimization steps:

Step 1. Optimize the ideal serial surfaces R by fixing S. By extracting the surfaces from the images of S and performing longitudinal surface registration [13], we obtain the current surface series R, and their longitudinal deformations $\mathbf{f}_k, k = 1, \ldots, K-1$. Then, R can be optimized using the finite gradient descent method:

$$R \leftarrow R - \xi \partial E(S,R)/\partial R, \tag{8}$$

where ξ is the updating step.

Step 2. Optimize the image sequences S by fixing R. We iterate all the axial images and re-assign each to the ith phase that gives the minimal energy function:

$$i = \text{argmin}_k\big(E(S,R)\big) = \text{argmin}_k\big(E(D|S) + \alpha E(S|R)\big). \tag{9}$$

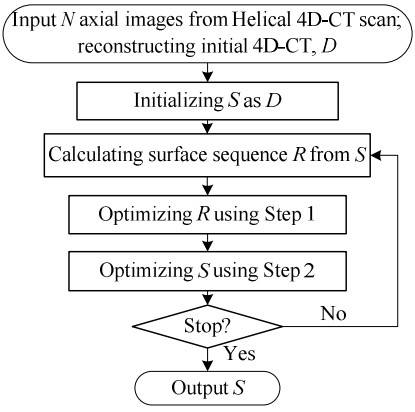

Fig. 1. The framework of the 4D-CT reconstruction algorithm

Notice that because of the nature of helical mode scanning, the distances between neighboring slices within each 3D CT image S_k are different. The surface registration method we used can register two surfaces with different meshes, and thus it can handle this issue. The optimization algorithm stops until the number of phase reassignment is smaller than a prescribed number (5 in our case), and the algorithm generally stops after 3-4 iterations. Fig. 1 summarizes the process of the algorithm.

3 Results

The datasets of thirty nine patients were used in the experiments. The data were collected using Philips Pinnacle³ in helical mode. The number of slices per scan is around 1330. Slice thickness is 3.0 mm, and pixel spacing in the X and Y directions is $1.17mm \times 1.17mm$. Elastic belt was used for monitoring the breath. Initial respiratory gating-based 4D-CT reconstruction was performed on the Pinnacle machine, which was used as the initialization of our algorithm. The datasets were then transferred to our workstation from PACS, and the proposed Bayesian 4D-CT reconstruction was applied to refine the results using a workstation running Microsoft Windows 7 professional with an Intel i7 CPU (2.30GHz) and 8.00 GB of RAM.

We compared the reconstruction results with two other methods. The first is the one reconstructed by the Pinnacle machine based on respiratory belt gating, and the second is the image matching-based image reconstruction proposed by Carnes *et al.* [10]. The Carnes algorithm first assigns manually the initial axial images into different respiratory phases and then uses slice-by-slice matching to sort the rest axial images. NCC is used as the image similarity measure. To automate this procedure, we used the assignment results of the first 20 axial images from the Pinnacle machine as the initialization of the Carnes algorithm. For our method, α and β were selected as 0.5 divided by the mean value of the corresponding energy functions. λ was selected so that the weight for temporal smoothness was half of the spatial smoothness. After reconstruction, we first visually assessed all the data. For the surrogate method, the artifacts of miss-assignment appeared more frequently, and we can also notice some

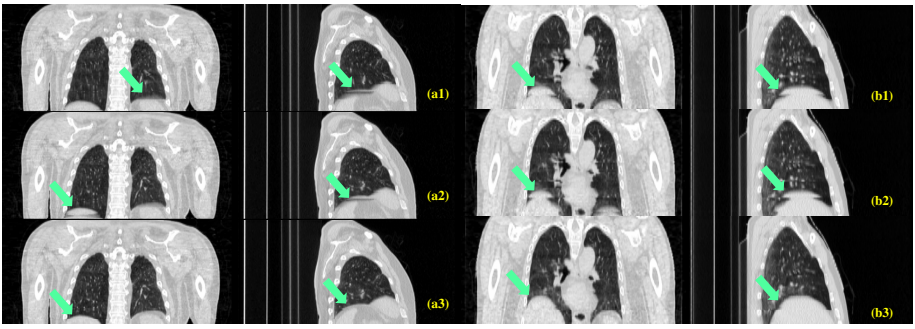

Fig. 2. Visual comparison of 4D-CT reconstruction results. Top: surrogate method; middle: Carnes algorithm; and bottom: the proposed Bayesian 4D-CT reconstruction.

similar discontinuity of the anatomical structures for the Carnes algorithm. Overall, the proposed Bayesian 4D-CT reconstruction preserved the anatomical structure in each 3D CT image much better. Fig. 2 illustrates some examples of the results. The top row shows the results of surrogate method, the middle row shows those of the Carnes algorithm, and the bottom row gives the reconstruction results of the proposed algorithm. Because the areas close to the diaphragm are subject to larger motion, we can notice the artifacts easily for the methods compared, and such motion artifacts have been corrected using the Bayesian 4D-CT reconstruction.

For quantitative comparison, we calculated the spatial and temporal smoothness about the chest surfaces and the lung field surfaces (extracted from the resultant CT images using [14]). Similar to Eq. (7), the spatial smoothness M_s of each subject is defined by the average absolute values of the surface gradients along z-direction,

$$M_s = \frac{1}{K}\sum_{k=1}^{K}\frac{1}{|\Omega|}\sum_{\mathbf{v}\in\Omega}|\partial R_k(\mathbf{v})/\partial z|. \tag{10}$$

The temporal smoothness M_T is calculated from the longitudinal deformation fields of the serial surfaces extracted:

$$M_T = \frac{1}{K-1}\sum_{k=1}^{K-1}\frac{1}{|\Omega|}\sum_{\mathbf{v}\in\Omega}|\mathbf{f}_{k+1}(\mathbf{v}+\mathbf{f}_k(\mathbf{v})) - \mathbf{f}_k(\mathbf{v})|. \tag{11}$$

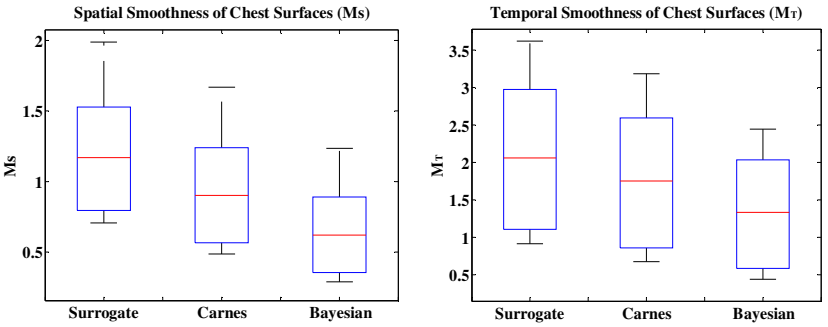

Fig. 3. Comparison of spatial and temporal smoothness of chest surfaces

Fig. 3 is the boxplot of the spatial and temporal smoothness of the chest surfaces for all 39 subjects in the experimental dataset. It can be seen that the proposed Bayesian 4D-CT reconstruction algorithm yielded more spatially and temporally smoother chest surfaces. Because we did not change the original axial images (only cubic B-Spline-interpolation was used), larger average smoothness value may indicate that there are more slices with artifacts in the reconstructed data. Therefore, the quantitative results indicate that there are less sudden jumps of the surfaces or less artifacts as compared to other methods. We also calculated the spatial and temporal smoothness of the lung fields extracted from the experimental results, and similar conclusion can be drawn from the boxplot shown in Fig. 4. It is worth noting that the spatial smoothness for lung field is bigger than that of the chest surface. This may indicate that chest surface is smoother and is suitable for applying the smoothness constraints.

Notice that the chest surface smoothness might be biased because it is also used in the energy function. Since the lung field surfaces were not used in the algorithm, the

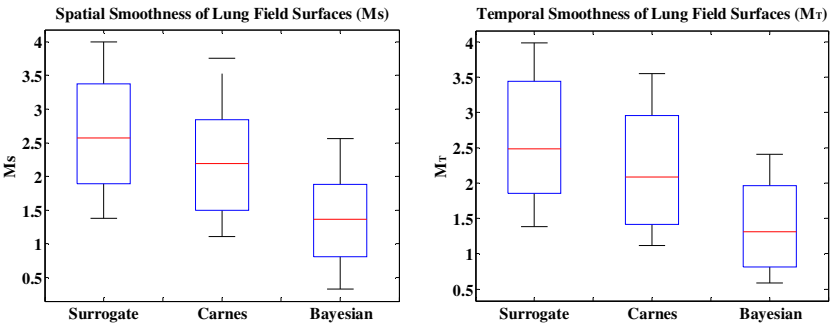

Fig. 4. Comparison of spatial and temporal smoothness of lung field surfaces

spatial and temporal smoothness metrics for the lung field surfaces extracted from the reconstructed images would be more appropriate. Due to the lack of ground truth of the 4D-reconstructed patient data, it is hard to conceive other relevant quantitative metrics at this point. In the future, we would like to further validate the quality of reconstruction using simulated images with known 4D-CT deformation patterns.

To further validate the results, all the reconstructed images were visually evaluated by two expert radiologists. Each image was visually assessed and the number of slices with artifacts (namely with noticeable sudden anatomical jumps) was counted. Fig. 5 illustrates the box plots of such numbers of slices with artifacts. The results confirmed the superiority of the proposed method as compared to others.

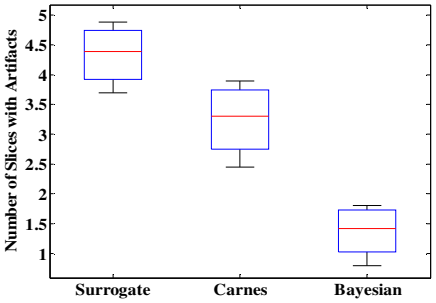

Fig. 5. Average numbers of slices with artifacts of 39 subjects

4 Conclusion

We proposed a Bayesian 4D-CT reconstruction algorithm for helical mode lung scanning. To preserve anatomical structures a joint Bayesian estimation is designed to ensure spatial and temporal smoothness of surfaces in the reconstructed 4D-CT images. Using clinical datasets for patients undergoing radiotherapy planning, we visually and quantitatively compared the performance of the proposed algorithm with the current surrogate and image-matching-based methods. The results showed that the

proposed algorithm yielded much less artifacts. In the future, we plan to incorporate vision-based chest surface monitoring devices in the framework for 4D-CT reconstruction on the fly.

References

1. Wu, G., Lian, J., Shen, D.: Improving image-guided radiation therapy of lung cancer by reconstructing 4D-CT from a single free-breathing 3D-CT on the treatment day. Medical Physics 39, 7694–7709 (2012)
2. Wink, N., Panknin, C., Solberg, T.D.: Phase versus amplitude sorting of 4D-CT data. Journal of Applied Clinical Medical Physics/American College of Medical Physics 7, 77–85 (2006)
3. Pan, T.: Comparison of helical and cine acquisitions for 4D-CT imaging with multislice CT. Medical Physics 32, 627–634 (2005)
4. Lu, W., Parikh, P.J., Hubenschmidt, J.P., Bradley, J.D., Low, D.A.: A comparison between amplitude sorting and phase-angle sorting using external respiratory measurement for 4D CT. Medical Physics 33, 2964–2974 (2006)
5. Ehrhardt, J., Werner, R., Saring, D., Frenzel, T., Lu, W., Low, D., Handels, H.: An optical flow based method for improved reconstruction of 4D CT data sets acquired during free breathing. Medical Physics 34, 711–721 (2007)
6. Johnston, E., Diehn, M., Murphy, J.D., Loo Jr., B.W., Maxim, P.G.: Reducing 4D CT artifacts using optimized sorting based on anatomic similarity. Medical Physics 38, 2424–2429 (2011)
7. Han, D., Bayouth, J., Song, Q., Bhatia, S., Sonka, M., Wu, X.: Feature guided motion artifact reduction with structure-awareness in 4D CT images. In: IEEE Conference on Computer Vision and Pattern Recognition (CVPR), pp. 1057–1064. IEEE (2011)
8. Zeng, R., Fessler, J.A., Balter, J.M., Balter, P.A.: Iterative sorting for 4DCT images based on internal anatomy motion. In: 4th IEEE International Symposium on Biomedical Imaging, pp. 744–747. IEEE (2007)
9. Li, R., Lewis, J.H., Cervino, L.I., Jiang, S.B.: 4D CT sorting based on patient internal anatomy. Physics in Medicine and Biology 54, 4821–4833 (2009)
10. Carnes, G., Gaede, S., Yu, E., Van Dyk, J., Battista, J., Lee, T.Y.: A fully automated non-external marker 4D-CT sorting algorithm using a serial cine scanning protocol. Physics in Medicine and Biology 54, 2049–2066 (2009)
11. Gianoli, C., Riboldi, M., Spadea, M.F., Travaini, L.L., Ferrari, M., Mei, R., Orecchia, R., Baroni, G.: A multiple points method for 4D CT image sorting. Medical Physics 38, 656–667 (2011)
12. Gerig, G., Jomier, M., Chakos, M.: Valmet: A new validation tool for assessing and improving 3D object segmentation. In: Niessen, W.J., Viergever, M.A. (eds.) MICCAI 2001. LNCS, vol. 2208, pp. 516–523. Springer, Heidelberg (2001)
13. Thomas Yeo, B.T., Sabuncu, M., Vercauteren, T., Ayache, N., Fischl, B., Golland, P.: Spherical demons: Fast surface registration. In: Metaxas, D., Axel, L., Fichtinger, G., Székely, G. (eds.) MICCAI 2008, Part I. LNCS, vol. 5241, pp. 745–753. Springer, Heidelberg (2008)
14. Zhu, X., Xue, Z., Gao, X., Zhu, Y., Wong, S.T.C.: Voles: Vascularity-Oriented Level Set Algorithm for Pulmonary Vessel Segmentation in Image Guided Intervention Therapy. In: IEEE International Symposium on Biomedical Imaging: From Nano to Macro, ISBI 2009, pp. 1247–1250. IEEE Press, Boston (2009)